Journal of Catalysis 364 (2018) 19–30

Contents lists available at ScienceDirect

Journal of Catalysis

journal homepage: www.elsevier.com/locate/jcat

A new molecular pathway allows the chemoselective reduction of nitroaromatics on non-noble metal catalysts

Reisel Millán, Lichen Liu, Mercedes Boronat *, Avelino Corma *

Instituto de Tecnología Química (UPV-CSIC), Universidad Politécnica de Valencia – Consejo Superior de Investigaciones Científicas, Avda. de los Naranjos s/n, 46022 Valencia, Spain

ARTICLE INFO

Article history:
Received 23 February 2018
Revised 2 May 2018
Accepted 3 May 2018

Keywords:
DFT
Mechanism
Nitroaromatics hydrogenation
Chemoselectivity
Non-noble metals

ABSTRACT

At difference with noble metals, the oxophylic character of non-noble metals strongly facilitates the rupture of the N—O bonds in nitrobenzene, yielding nitrosobenzene as primary reaction intermediate. By combining periodic DFT calculations and kinetic studies, a direct pathway involving successive dissociation of N—O bonds followed by two hydrogenation steps, Ph-NO_2 → Ph-NO → Ph-N → Ph-NH → Ph-NH_2, has been found as most favorable on Ni catalysts. The rate determining step of the global process is the hydrogen transfer to adsorbed Ph-N intermediate. The catalyst surface becomes partly oxidized during reaction, which favors the vertical adsorption of the nitroaromatic compounds and enhances selectivity, while total surface oxidation leads to catalyst deactivation. It is proposed that both catalytic activity and selectivity of Ni and, possibly, other non-noble metals can be tuned by controlling the degree of oxidation of the metal surface.

1. Introduction

The industrial production of chemical compounds such as pharmaceuticals, agrochemicals, polymers and dyes often use functionalized anilines as reactants [1]. The synthesis of these aniline derivatives is commercially carried out by selective reduction of substituted nitroaromatics, i.e., nitroaromatics containing other reducible functional groups that must remain unaffected during the reaction, using stoichiometric amounts of reducing agents like Fe, Mn, Sn, Zn or S compounds, with the associated production of waste. For environmental reasons, the selective catalytic hydrogenation of nitroaromatic compounds has been widely investigated in the last years, and heterogeneous catalysts based on supported noble metals like Pd, Pt, Ru, Rh or Ir, and on Ni have been developed, the most effective being Raney Ni, Fe- and Cu-promoted 5% Ir/C, or 1% Pt/C. The catalytic hydrogenation becomes especially challenging when C=C, C≡C or C≡N are present in the molecule, and in this case addition of modifiers or promoters like Pb, H_3PO_2, $FeCl_2$ or V complexes is required [2,3]. A different approach consists of taking advantage of particle size effects and strong metal support interactions to prepare highly selective catalysts by dispersing noble metals like Au, Ru or Pt on reducible oxides like TiO_2 and Fe_2O_3 [4–10]. It has been shown that, in this case, the high chemoselectivity achieved is due to the adsorption of the substituted nitroaromatic on the metal oxide support preferentially through the nitro group, thus avoiding the hydrogenation of the other reducible groups that are kept far from the catalyst surface.

However, due to the high cost of noble metals, there is an increasing interest to achieve the same catalytic performance using non-noble metals. In this line, interesting results have been reported with Co_3O_4 and Fe_2O_3 nanoparticles supported on carbon fibers or surrounded by N-doped carbon materials, which control the activity and selectivity of the catalysts [11–14], and with Co nanoparticles covered by carbon (Co@C) capable of selectively reduce nitroarenes under mild conditions [15]. Other non-noble metal based catalysts such as Ni [16–18] as well as Ni—Co and Ni—Fe alloys have also been investigated with good results [18–20].

All this previous work, though significant regarding catalyst performance, has not provided yet a clear picture of the molecular mechanism, which is still based on the macroscopic mechanism proposed by Haber [21] in 1898 for the hydrogenation of nitrobenzene (see Scheme 1). According to Haber's mechanism, there are two possible pathways for the reduction of the nitro group, regardless the type of catalyst. The direct route involves the formation of nitrosobenzene (Ph-NO), phenylhydroxylamine (Ph-NHOH) and finally aniline (Ph-NH_2), following three consecutive hydrogenation steps. The second pathway, commonly named indirect or condensation route, involves the condensation of nitrosobenzene and phenylhydroxylamine to form the azoxy intermediate

* Corresponding authors.
E-mail addresses: boronat@itq.upv.es (M. Boronat), acorma@itq.upv.es (A. Corma).

https://doi.org/10.1016/j.jcat.2018.05.004
0021-9517/

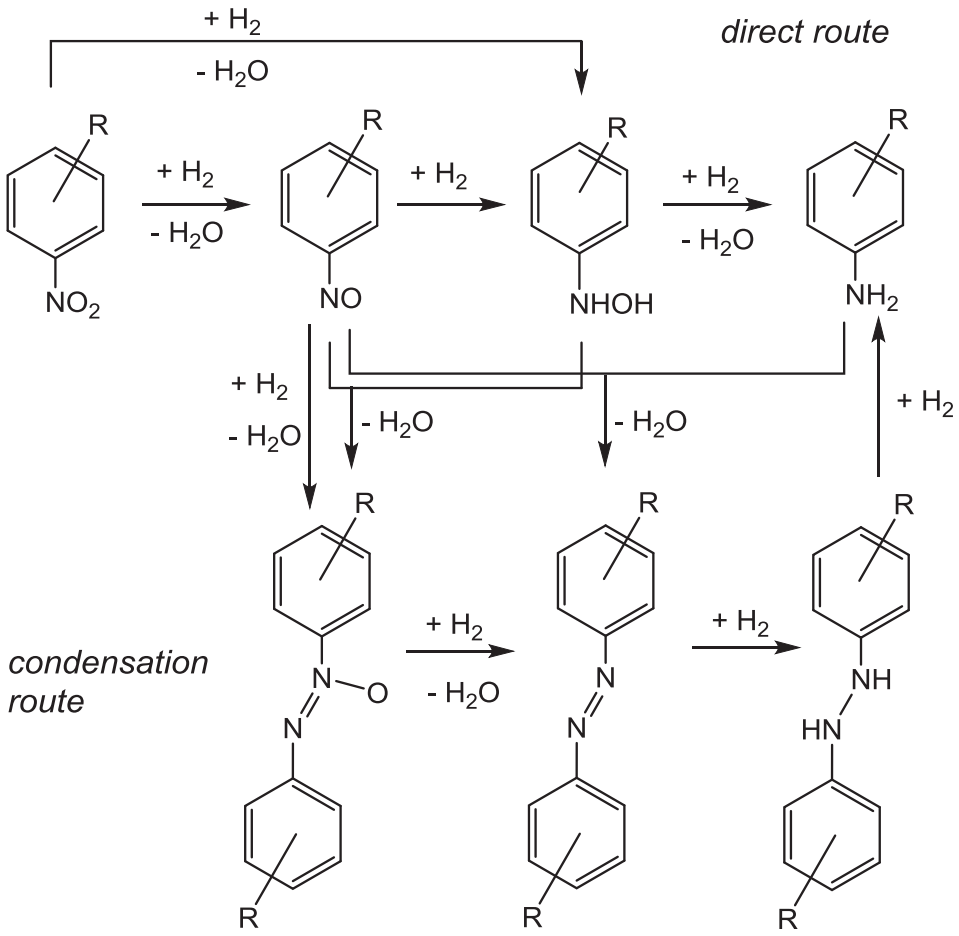

Scheme 1. Mechanism of hydrogenation of the nitro group in nitroaromatics.

(Ph-N=NO-Ph) which then follows the sequence azo (R—N=N—R), hydrazo (R—NH—NH—R) and finally aniline. While this mechanism is generally accepted, some modifications have been suggested. For example, Gelder et al. concluded that nitrosobenzene is not a reaction intermediate in the direct route to aniline on Pd or Raney Ni catalysts, and proposed instead an adsorbed Ph-NOH species as the true intermediate [22]. Corma et al. confirmed that a direct route from nitrobenzene to phenylhydroxylamine can also contribute to the production of aniline from nitrobenzene on Au/TiO_2 [23]. The pathway through which the reaction proceeds depends not only on the type of catalyst, but also on the experimental conditions, since at low H_2 pressure nitrosobenzene was detected on a Raney Ni catalyst [22].

Despite the relevance of this reaction and the questions still open regarding its mechanism, only a few studies on the molecular reaction mechanism addressing all the elementary steps of the reaction pathway have been reported [24–26], the rest focusing on the adsorption of the nitroaromatic reactant as a key factor to explain the selectivity of the reduction of nitrobenzene and its derivatives [27,28]. Sheng et al. [24] reported that the preferential path for the reduction of nitrobenzene on Pt(1 1 1) surface is the double H-induced dissociation of the N—O bonds of the nitro group via a $R\text{-}N(OH)_2$ intermediate, and that the most energy demanding step is the dissociation of the N—O bond. Zhang et al. [25] studied the reduction of nitrobenzene on a bimetallic Pd_3Pt(1 1 1) system and identified the Pd-top-top site as the most favorable for vertical adsorption of nitrobenzene, but they did not considered parallel adsorption geometries. As regards non-noble metals, Mahata et al. [26] studied the direct and indirect routes for the reduction of nitrobenzene on Ni(1 1 1) surface considering the same elementary steps previously reported for Pt(1 1 1), and concluded that the direct route is more favorable than the indirect one, although the reaction may proceed via both pathways. Surprisingly, the same mechanism is generally assumed for noble and non-noble metals, and the higher oxophilicity and lower reducibility of Ni and other non-noble metals as compared to Pt are not usually taken into account. For this reason, we have carried out here a detailed mechanistic study of the reduction of nitrostyrene on a non-noble Ni catalyst using H_2 as reducing agent. The combination of theoretical and kinetic work has resulted in a new mechanistic proposal that differs from that observed for noble metals, and which can explain how the chemoselective hydrogenation of nitroaromatics occurs on Ni under mild reaction conditions. From these results, it is outlined how Ni based catalysts should be synthesized to maximize activity and chemoselectivity.

2. Experimental section

2.1. Computational details

Periodic density functional calculations were performed using the Perdew-Wang (PW91) exchange-correlation functional within the generalized gradient approach (GGA) [29,30] as implemented in the VASP code [31]. The valence density was expanded in a plane wave basis set with a kinetic energy cutoff of 450 eV, and the effect of the core electrons in the valence density was taken into account

by means of the projected augmented wave (PAW) formalism [32]. This computational setup has been previously used to study H_2 activation and nitrobenzene hydrogenation on Au and Pt based catalysts [5,7]. All calculations are spin polarized. The atomic positions were optimized by means of a conjugate-gradient algorithm until atomic forces were smaller than 0.01 eV/Å. Transition state structures were located using the DIMER algorithm [33,34], and vibrational frequencies were calculated numerically. Dispersion energies were evaluated using the D3 Grimme's method. [35]

The catalyst surface was simulated by means of a supercell slab model consisting of five atomic layers oriented along the (1 1 1) plane, which is the most stable and preferentially exposed in metal catalysts, and separated by a vacuum region of 10 Å to avoid interaction between periodically repeated slabs. The size of the supercell slab was also large enough to avoid interaction between the periodically repeated adsorbates. Thus, two different supercell slab sizes (2×2, and 3×3) were used to model H_2 dissociation at different hydrogen coverages, using converged Monkhorst-Pack *k*-points [36] meshes of $6 \times 6 \times 1$ and $3 \times 3 \times 1$, respectively.

The study of the adsorption of nitrostyrene on the catalyst surface and of the reaction mechanism required a large 4×6 supercell slab containing 120 Ni atoms, and integration in the reciprocal space was carried out at the Γ k-point of the Brillouin zone. Due to the high computational cost of the mechanistic study, it was performed using styrene to investigate the hydrogenation of the vinyl group, and nitrobenzene to study the reduction of the nitro group. During the geometry optimizations the atomic positions of the adsorbates and of the Ni atoms in the two uppermost layers were allowed to fully relax, while the Ni atoms in the three bottom layers were kept fixed at their bulk optimized positions. For each system, interaction (E_{int}), activation (E_{act}) and reaction (ΔE) energies were calculated as:

$$E_{int} = E(slab - adsorbate) - E(slab) - E(adsorbate)$$

$$E_{act} = E(TS) - E(R)$$

$$\Delta E = E(P) - E(R)$$

where E(slab-adsorbate), E(slab) and E(adsorbate) are the total energies of the optimized Ni(1 1 1)-adsorbate complex, clean Ni(1 1 1) surface model and isolated adsorbate molecule, respectively, including the ZPE correction. For each elementary step considered, E(R), E(TS) and E(P) are the total energies of the corresponding reactant complex, transition state and product, respectively, including the ZPE correction. Unless stated otherwise, all energy values mentioned in the text are ZPE-corrected.

Equilibrium K_{eq} and kinetic rate k_r constants for the most relevant steps were derived from calculated reaction ΔG and activation ΔG_{act} Gibbs free energies, as follows:

$$K_{eq} = e^{-\Delta G/RT}$$

$$k_r = \left(\frac{k_B T}{h}\right) e^{-\Delta G_{act}/RT}$$

The absolute Gibbs free energies of all species are given by:

$$G = E_{tot} + E_{zpe} + RT + E_{vib} - TS_{vib}$$

where E_{tot} is the electronic energy obtained from the DFT calculation, E_{zpe} is the zero point energy correction, E_{vib} is the vibrational thermal energy contribution and S_{vib} is the vibrational entropy. The zero-point energy corrections and the vibrational contributions to the energy and entropy were calculated according to:

$$E_{zpe} = \sum_{i=1}^{3N-6} \frac{1}{2} h\upsilon_i$$

$$E_{vib} = R \sum_{i=1}^{3N-6} \frac{h\upsilon_i}{k_B(e^{h\upsilon_i/k_B T} - 1)}$$

$$S_{vib} = R \sum_{i=1}^{3N-6} \left[\frac{h\upsilon_i}{k_B T(e^{h\upsilon_i/k_B T} - 1)} - ln(1 - e^{h\upsilon_i/k_B T})\right]$$

using the vibrational frequencies υ obtained from the DFT calculations. In the case of gaseous molecules the rotation and translational contributions to the entropy and energy were also included in the calculation of the free energy as follows:

$$G = E_{tot} + E_{zpe} + E_{vib} + E_{rot} + E_{trans} + RT - T(S_{vib} + S_{rot} + S_{trans})$$

where $E_{rot} = E_{trans} = 3/2RT$, and the rotational and translational contributions to the entropy are given by:

$$S_{rot} = R\left\{ln\left[\frac{\sqrt{\pi I_A I_B I_C}}{\sigma}\left(\frac{2\Pi k_B T}{h^2}\right)^{3/2}\right] + \frac{3}{2}\right\}$$

$$S_{trans} = R\left\{ln\left[\left(\frac{2\Pi M k_B T}{h^2}\right)^{3/2} V\right] + \frac{3}{2}\right\}$$

2.2. Catalytic tests

The chemoselective hydrogenation of nitroarenes was performed in batch reactor. The reactant, internal standard (dodecane), solvent (toluene), catalyst, as well as a Teflon lined magnetic bar were added into the batch reactor of 7.5 mL volume. After the reactor was sealed, air was purged by flushing five times with 10 bar of hydrogen. Then the autoclave was pressurized with H_2 to the corresponding pressure (2–12 bar). The stirring speed was kept at 1100 rpm and the size of the catalyst powder was below 0.05 mm to avoid external and internal diffusion limitations, respectively. Finally, the batch reactor was heated to the target temperature (20–150 °C). For the kinetic studies, 50 μL of the mixture was taken out for GC analysis at different reaction times. All products were detected and quantified by GC and GC–MS. GC analyses were performed in an instrument equipped with a 25 m capillary column of 5% phenylmethylsilicone. GC–MS analyses were performed on a spectrometer equipped with the same column as for the GC and operated under the same conditions.

3. Results and discussion

3.1. Theoretical study

3.1.1. Hydrogen activation

The first step considered was the adsorption and dissociation of molecular H_2 at different sites on the Ni(1 1 1) surface model. In agreement with previous theoretical studies on this process [26,37], molecular H_2 adsorbs on-top of a Ni atom, and its H-H bond length increases from 0.75 Å to 0.88 Å, indicating a certain degree of activation (see Fig. S1). Rupture of this bond involves a very low activation barrier (see Table S1), and after dissociation the two H atoms occupy *fcc* and *hcp* hollow sites on the catalyst surface. The process is highly exothermic, with the adsorption energy per H atom (E_{ads}/H in Table S1) being around −13 kcal/mol at low coverages ($\theta = 0.22$ and $\theta = 0.5$), and slightly lower at full coverage $\theta = 1$. The dissociation of H_2 on a Ni(1 1 1) surface already covered by H was also considered (see Fig. S1, bottom). The activation energy increases by ~2 kcal/mol and the reaction is less exothermic, but it is still a kinetically and thermodynamically favorable process.

3.1.2. Nitrostyrene adsorption

According to previous studies [5–10], the mode of adsorption of the functionalized nitroaromatic compound on the catalyst surface determines the selectivity of the process. The two adsorption geometries considered in this study, namely parallel (P) and vertical or perpendicular to the metal surface (V), are shown in Fig. 1. In the parallel adsorption fashion all functional groups of nitrostyrene are interacting with the catalyst surface, with optimized Ni—O distances of 2.06 and 2.04 Å, and Ni—C distances between 2.00 and 2.32 Å. Due to these metal-substrate interactions, the C=C bond lengths in the aromatic ring increase by 0.05 Å, the C=C bond of the vinyl group is elongated 0.1 Å, and both N—O distances increase by 0.9 Å as compared to the gas phase or isolated molecule. In addition, the H atoms of the C—H bonds lie slightly above the aromatic ring plane, indicating that the hybridization of the vinyl and phenyl C atoms has changed from sp^2 to sp^3 and nitrostyrene is in a chemisorbed state. In contrast, and despite the optimized Ni—O distances are shorter in the vertical adsorption fashion, 1.95 Å, the geometrical parameters of the aromatic and vinyl groups don't change, and only the N—O bonds are elongated 0.05 Å.

The calculated adsorption energies listed in Table S3, −37.3 and −17.0 kcal/mol for the P and V orientations, respectively, reflect the geometrical differences described above and suggest that nitrostyrene will preferentially adsorb in the parallel mode on a clean Ni(1 1 1) surface. To check the validity of the slab model employed, nitrostyrene was also adsorbed in P orientation on a larger 6x6 supercell slab containing 180 Ni atoms. The calculated interaction energy, −35.0 kcal/mol (not ZPE corrected) is similar to that obtained on the 6x4 supercell slab model, −33.9 kcal/mol without ZPE correction, confirming that the model used is large enough to study this reaction. The presence of co-adsorbed H atoms weakens the interaction of nitrostyrene with the Ni surface in parallel orientation without significantly modifying the vertical adsorption, so that similar interaction energy values are obtained for the P and V orientations, −16.7 and −15.5 kcal/mol, respectively, at a 0.5H coverage (see Table S3). And a similar effect is observed when the catalyst surface is partly covered with O atoms that are detached from the nitro group in the course of the reaction, as will be explained later. Inclusion of dispersion energies by means of Grimme's D3 method greatly increases the calculated interaction energy values (see Table S3), especially in the P orientation, but still a trend is observed indicating that the presence of adsorbed species on the Ni surface destabilizes parallel adsorption modes without modifying too much the vertical adsorption modes.

3.1.3. Reduction of vinyl group

The competitive hydrogenation of the C=C double bond in nitrostyrene, which would lead to a low selectivity towards the desired vinyl-aniline, was investigated in first place using styrene as model substrate. The optimized geometries of all structures involved in the mechanism are shown in Fig. 2 together with the calculated energy profile. The initial reactant system (R) contains one styrene molecule co-adsorbed on the Ni(1 1 1) surface with two H atoms occupying hollow positions, and the complete process consists of two hydrogen transfer steps to the C=C carbon atoms.

In all optimized structures, both minima and transition states, the aromatic ring keeps the same adsorption geometry, with all C atoms directly interacting with surface Ni atoms. The C=C bond length of the vinyl group increases from 1.42 Å in adsorbed styrene to 1.45 Å in TS1, and 1.52 in the reaction intermediate INT, in TS2 and in the ethylbenzene product. The optimized length of the C—H bond being formed in TS1 is 1.39 Å, and 1.50 Å in TS2. Both steps are energetically similar, slightly endothermic (6.3 and 7.1 kcal/mol for the first and second H transfer, respectively) and involving activation energy barriers of ∼14 kcal/mol (see Table S4). Finally, desorption of the ethylbenzene product is endothermic by 20.4 kcal/mol (see Table S6). The calculated equilibrium K_{eq} and kinetic rate k_r constants summarized in Table S5 indicate that hydrogenation of the C=C bond is not thermodynamically favored on Ni, and its rate will strongly depend on the concentration of reactants, styrene and H_2.

3.1.4. Reduction of nitrobenzene

The mechanism of reduction of the nitro group in substituted nitroaromatics was investigated using nitrobenzene as model substrate. The initial reactant structure consists of a nitrobenzene molecule adsorbed either parallel (P) or vertical (V) on a Ni(1 1 1) slab model pre-covered with 6H atoms placed at hollow sites. The elementary steps considered and their calculated activation and reaction energies are summarized in Table 1. The optimized geometries of the intermediate and transition state structures involved in the P and V pathways are depicted in Figs. 3 and 4, respectively, and the calculated energy profiles are illustrated in Figs. 5 and 6. Taking into account the results presented by Mahata et al. [26] showing that on Ni(1 1 1) the direct route is more favorable, condensation pathways have not been considered in this work.

3.1.4.1. Parallel pathways. According to previous studies on Ni(1 1 1) and Pt(1 1 1) [24–26], the reaction starts with the transfer

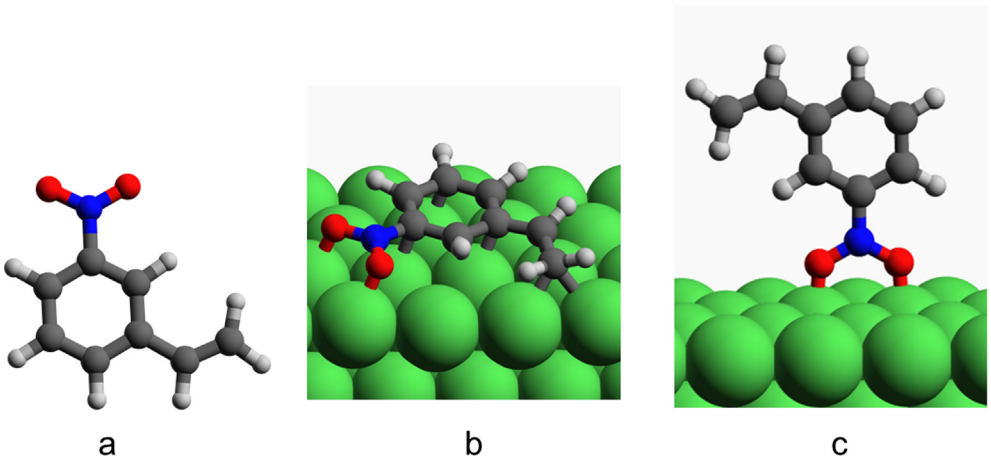

Fig. 1. Optimized geometry of nitrostyrene: (a) isolated molecule, (b) parallel adsorption and (c) vertical adsorption on Ni(1 1 1) surface. Ni, C, N, O and H atoms are depicted as green, gray, blue, red and white balls, respectively. Optimized bond lengths are given in Å.

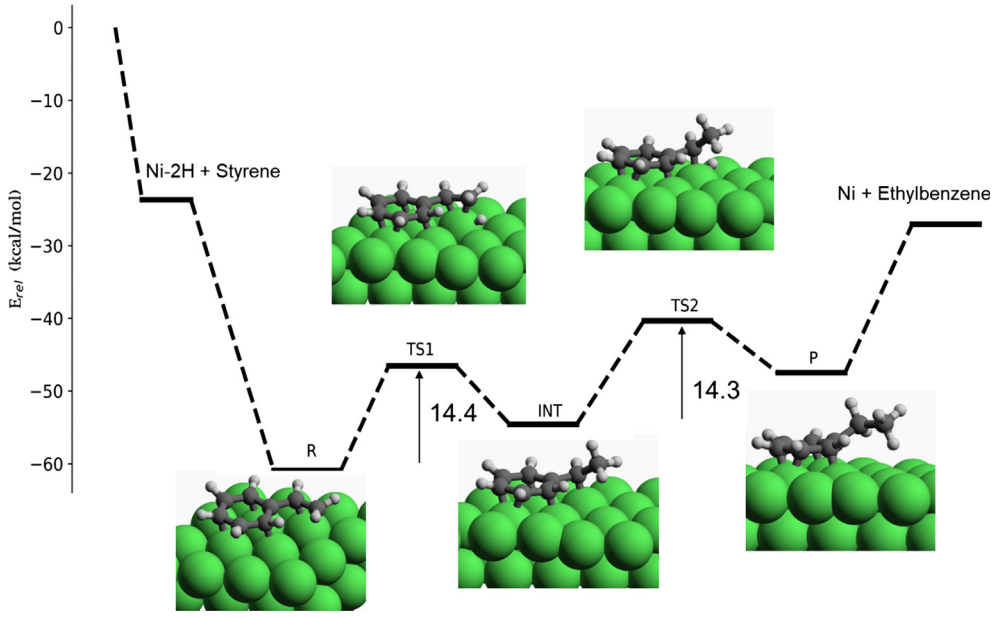

Fig. 2. Optimized structures and calculated energy profile for the hydrogenation of the C=C bond in styrene on a Ni(1 1 1) surface. The zero energy level corresponds to the sum of the ZPE-corrected energies of the Ni slab + H_2 + Styrene.

Table 1
Calculated reaction and activation energies for all elementary steps of the reduction of nitrobenzene on Ni(1 1 1) surface with parallel (P) and vertical (V) geometries. Activation energies are given for the forward ($E_{act}f$) and reverse process ($E_{act}r$). All energies include ZPE correction and are given in kcal/mol.

Step	Reaction	Parallel			Vertical		
		$E_{act}f$	ΔE	$E_{act}r$	$E_{act}f$	ΔE	$E_{act}r$
1 → 2	C_6H_5-NO_2 + H* → C_6H_5-NOOH	13.5	−1.3	14.8	23.6	22.2	1.4
2 → 3	C_6H_5-NOOH + H* → C_6H_5-$N(OH)_2$	20.1	11.3	8.9	17.8	1.8	16.0
3 → 5	C_6H_5-$N(OH)_2$ → C_6H_5-NOH + OH	4.0	−35.0	39.0	3.2	−32.2	35.4
2 → 5	C_6H_5-NOOH → C_6H_5-NOH + O*	7.0	−28.3	35.2			
5 → 6	C_6H_5-NOH → C_6H_5-N + OH*	5.3	−29.9	35.2			
5 → 7	C_6H_5-NOH + H* → C_6H_5-NHOH	27.2	13.1	14.1	23.9	6.9	17.0
6 → 8	C_6H_5-N + H* → C_6H_5-NH	23.5	−1.5	25.0	22.4	15.4	7.0
7 → 8	C_6H_5-NHOH → C_6H_5-NH + OH**	9.7	−30.9	40.6	3.9	−32.0	35.9
8 → 9	C_6H_5-NH + H* → C_6H_5-NH_2	21.6	2.3	19.3	19.4	−0.4	19.8
1 → 4	C_6H_5-NO_2 → C_6H_5-NO + O*	7.1	−31.8	38.9	9.2	−15.0	24.2
4 → 5	C_6H_5-NO + H* → C_6H_5NOH	15.7	7.1	8.6	19.9	6.8	13.1
4 → 6	C_6H_5-NO → C_6H_5-N + O**	14.0	−22.8	36.8	7.1	−38.7	45.8
4 → 10	C_6H_5-NO + H* → C_6H_5NHO	20.7	4.3	16.4			
10 → 7	C_6H_5-NHO + H* → C_6H_5-NHOH	17.0	8.2	8.8			
10 → 8	C_6H_5-NHO → C_6H_5-NH + O*	6.7	−34.7	41.4			

of a H atom from the Ni(1 1 1) surface to one of the O atoms of the nitro group in adsorbed nitrobenzene (structure P-1 in Fig. 3), leading to formation of a C_6H_5-NOOH intermediate (structure P-2). The O—H distance in the transition state structure P-TS1-2 is 1.47 Å, and the N—O bond length increases from 1.32 to 1.39 Å in this process. The calculated activation and reaction energies are 13.5 and −1.3 kcal/mol, respectively (step 1 → 2 in Table 1). In principle, there are two possible steps starting from C_6H_5-NOOH (P-2), either a second hydrogen transfer to the other O atom of the nitro group to form C_6H_5-$N(OH)_2$ (structure P-3) or direct N—OH bond breaking yielding nitrosobenzene C_6H_5-NO (structure P-4). In agreement with previous studies [26], every attempt to find a transition state corresponding to N—OH breaking and hydroxyl release to the catalyst surface, assisted or not by adsorbed H, failed, and therefore we rather continued with the second possibility: hydrogen transfer. The activation and reaction energies obtained for the hydrogen transfer to the second O atom in P-2 are 20.1 kcal/mol and 11.3 kcal/mol respectively (step 2 → 3 in Table 1) being this step less favorable kinetically and thermodynamically than the first one.

The optimized N—O bond lengths in reaction intermediate C_6H_5-$N(OH)_2$ (structure P-3 in Fig. 3) are 1.43 Å, indicating that both N—O bonds have been activated and therefore could be more easily broken in the next elementary step (step 3 → 5 in Table 1). Indeed, the calculated activation barrier is low, 4.0 kcal/mol, and the process is clearly exothermic, −35.0 kcal/mol, despite the fact that a strong N—O bond is being broken. The optimized N—O and O—Ni distances in the transition state P-TS3-5 are 1.70 and 2.06 Å, respectively. The simultaneous formation of a stable O—Ni bond as the OH group is released from intermediate P-3 overcompensates the energy required to dissociate the N—O bond, which is not an unexpected behavior taking into account the oxophilic character of Ni [38].

In fact, the activation of the second O atom in intermediate P-2 by hydrogen transfer is not even necessary, and a favorable pathway exists (step 2 → 5 in Table 1) to directly break the N—O bond through transition state P-TS2-5 generating the same C_6H_5-NOH intermediate obtained through steps 1 → 2 and 2 → 3 (structure P-5 in Fig. 3). The calculated activation energy for this process is

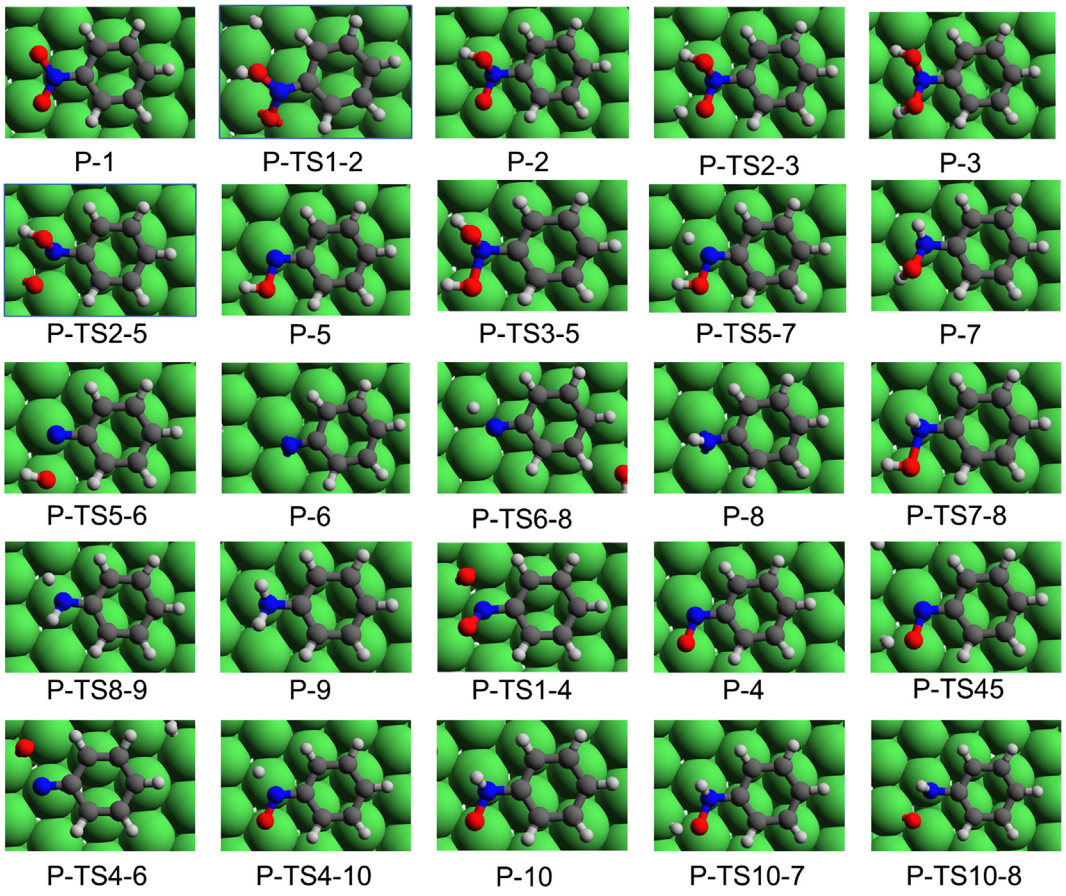

Fig. 3. Optimized structures of minima and transition states involved in the parallel mechanism of nitrobenzene reduction over Ni(1 1 1) surface.

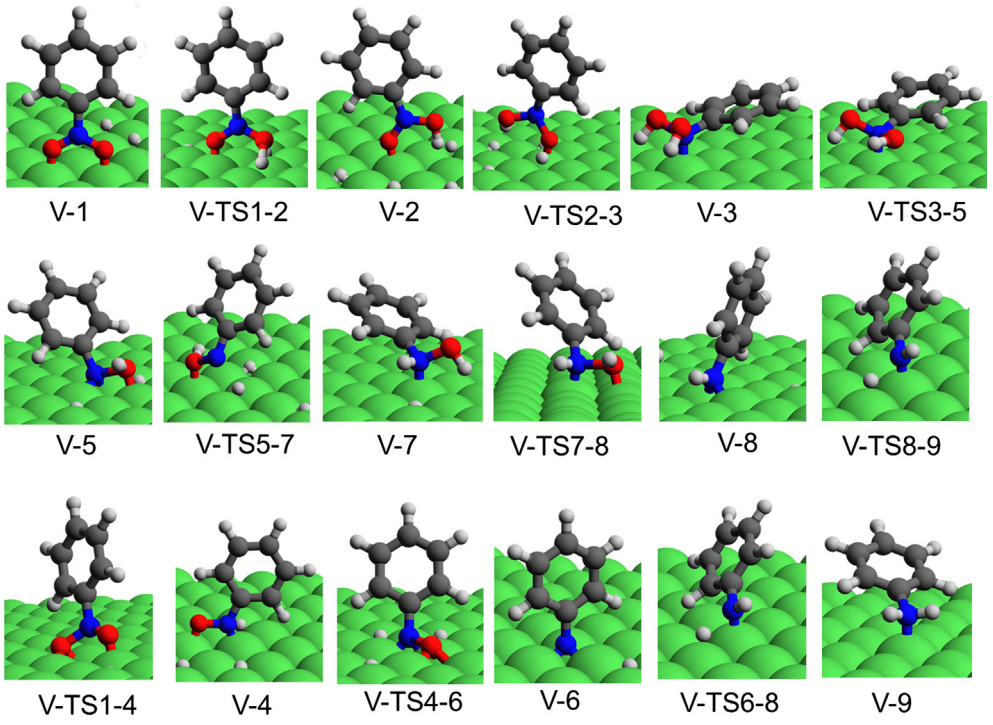

Fig. 4. Optimized structures of minima and transition states involved in the vertical mechanism of nitrobenzene reduction over Ni(1 1 1) surface.

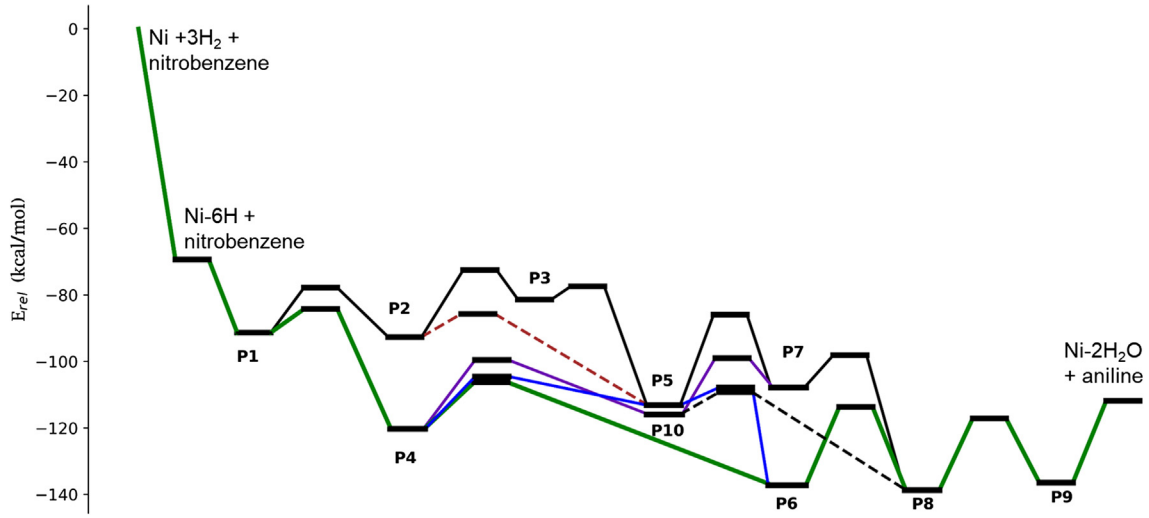

Fig. 5. Calculated energy profile for the parallel pathways for nitrobenzene reduction over Ni(1 1 1) surface. The zero energy level corresponds to the sum of the ZPE-corrected energies of the Ni slab + $3H_2$ + Nitrobenzene.

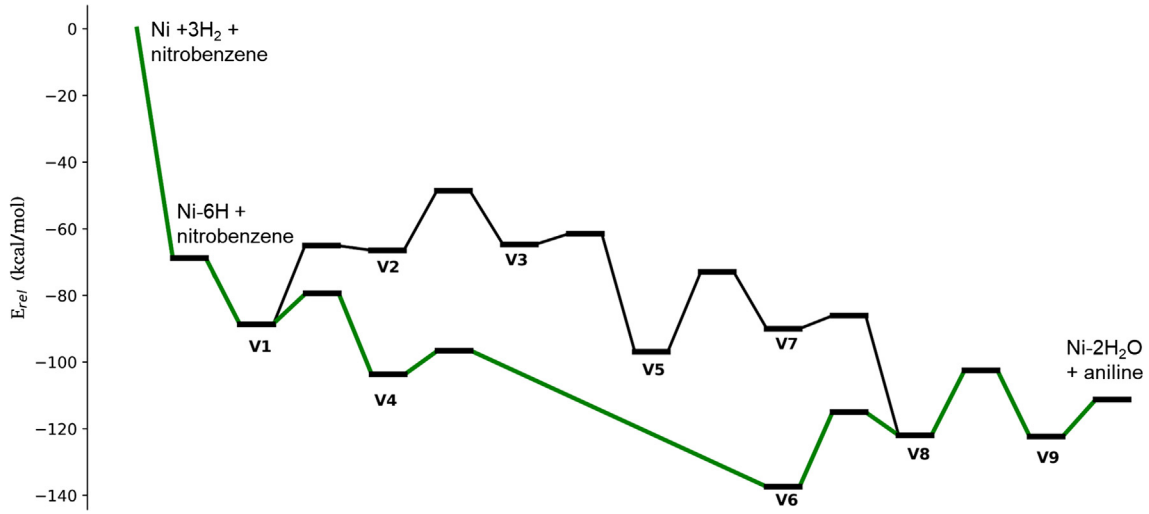

Fig. 6. Calculated energy profile for the vertical pathways for nitrobenzene reduction over Ni(1 1 1) surface. The zero energy level corresponds to the sum of the ZPE-corrected energies of the Ni slab + $3H_2$ + Nitrobenzene.

7.0 kcal/mol, significantly lower than the value obtained for step 2 → 3 (20.1 kcal/mol), and −28.3 kcal/mol are released in this reaction.

Again, two possible pathways start from C_6H_5-NOH or P-5 intermediate: N—O bond cleavage leading to a C_6H_5-N species (P-6 in Fig. 3) and adsorbed hydroxyl (step 5 → 6 in Table 1), or hydrogen transfer to the N atom leading to formation of a C_6H_5-NHOH structure (P-7 in Fig. 3), according to reaction 5 → 7 in Table 1. Again, the activation barrier for the N—O bond breaking (5.3 kcal/mol) is much lower than that for the hydrogen transfer (27.2 kcal/mol). Moreover, the former process is very exothermic (−29.9 kcal/mol) while the latter is endothermic (13.1 kcal/mol). The global energy profile plotted in Fig. 5 shows the higher stability of the C_6H_5-N intermediate, which can be explained by the strong coordination of N to two Ni atoms of the catalyst surface, with optimized N—Ni distances of 1.88 Å. Two additional hydrogen transfer steps (reactions 6 → 8 and 8 → 9 in Table 1) yield adsorbed C_6H_5-NH intermediate (P-8 in Fig. 3) and finally aniline (P-9 in Fig. 3), both involving high activation energy barriers (23.5 and 21.6 kcal/mol, respectively). On the other hand, structure P-8 can also be formed by direct dehydroxylation of intermediate P-7 releasing 30.9 kcal/mol and involving an activation energy of 9.7 kcal/mol (step 7 → 8 in Table 1).

So far, a complete pathway for nitrobenzene reduction to aniline has been described which does not include the formation of nitrosobenzene (C_6H_5-NO), a species that has been proposed as reaction intermediate in the direct route when Ni is used as catalyst [15]. Taking into account the oxophylic character of Ni and the observation that the formation of Ni—O bonds compensates the rupture of the N—O bonds in steps 3 → 5, 2 → 5, 5 → 6 and 7 → 8, we considered at this point the formation of nitrosobenzene (P-4) by direct dissociation of one of the two N—O bonds in nitrobenzene (P-1). Interestingly, the calculated activation energy for this process (step 1 → 4 in Table 1), 7.1 kcal/mol, is much lower than that found for the hydrogenation step 1 → 2, and the reaction is highly exothermic. The set of elementary steps following the formation of nitrosobenzene are similar to those described so far. Hydrogenation of either the O or the N atom in P-4, steps 4 → 5 and 4 → 10, respectively, are slightly endothermic and involve activation energies close to 20 kcal/mol, while direct dissociation

of the N—O bond yielding the previously described C_6H_5-N intermediate (P-6) is clearly exothermic and involves a lower activation barrier of 14.0 kcal/mol.

The energy profile for the whole sequence is plotted in Fig. 5, and clearly evidences that the preferred pathway for nitrobenzene hydrogenation on Ni(1 1 1) (green line) is, at difference with Pt(1 1 1), the following: Ph-NO_2 → Ph-NO → Ph-N → Ph-NH → Ph-NH_2 (or 1 → 4 → 6 → 8 → 9 according to the labeling in this work). This short route consists of two fast and highly exothermic N—O bond dissociation steps followed by two almost thermoneutral H transfers to N.

3.1.4.2. Vertical pathways. The study of the mechanism of the reduction of nitrobenzene adsorbed in a vertical orientation is critical to understand and to try to improve the selectivity of the reaction. The elementary steps involved (Table 1) and the intermediate and transition state structures found (Fig. 4) are similar to those described for the parallel pathways, except for the fact that in the vertical orientation the aromatic ring is not interacting with the Ni surface.

Starting from nitrobenzene adsorbed perpendicular to the Ni(1 1 1) surface (structure V-1 in Fig. 4), the first hydrogen transfer yielding a C_6H_5-NOOH intermediate (structure V-2) involves an activation energy barrier of 23.6 kcal/mol, that is, 10 kcal/mol higher than the value obtained for the same step with a parallel geometry. In addition, the reaction intermediate V-2 is very unstable because it is only bonded to the Ni surface through one oxygen atom, so that elementary step 1 → 2 is highly endothermic (22.2 kcal/mol) and therefore unfavorable both kinetically and thermodynamically. The search for a minimum structure for C_6H_5-NOOH intermediate with the two O atoms interacting with the Ni atoms of the surface always resulted in dissociation of the N—O bond yielding nitrosobenzene C_6H_5-NO and an OH group adsorbed on hollow sites, but again no transition state could be optimized for this step. The activation energy obtained for the hydrogen transfer to the second O atom in structure V-2 (step 2 → 3 in Table 1) is also high, 17.8 kcal/mol, and the reaction is slightly endothermic. The optimized geometry of structure V-3 is not completely perpendicular to the Ni surface (see Fig. 4). Only the N atom is directly attached to a Ni atom, with an optimized Ni—N distance of 2.11 Å, while the aromatic ring is forming an angle of ~23.4° with the metal surface. Breaking an N—O bond in this structure (step 3 → 5 in Table 1) involves a low activation energy of 3.2 kcal/mol and is exothermic by 32.2 kcal/mol, due to the formation of two Ni—O bonds in structure V-5 (see Fig. 4).

On the other hand, formation of nitrosobenzene V-4 directly from nitrobenzene V-1 (step 1 → 4 in Table 1) is again the preferred pathway, with an activation energy of only 9.2 kcal/mol and with 15.0 kcal/mol being released in this step. Further dissociation of the N—O bond in C_6H_5-NO yielding the C_6H_5-N intermediate (structure V-6 in Fig. 4) is also favored in the vertical orientation, since the activation energy for step 4 → 6 drops to 7.1 kcal/mol and the reaction is exothermic by 38.7 kcal/mol. The calculated activation energy for step 7 → 8 involving N—O bond breaking is also lower in the vertical pathway, while the activation barriers for hydrogen transfer steps are similar to those found in the parallel pathways, around 20 kcal/mol range. Notice, however, that the first H transfer to C_6H_5-N intermediate generating C_6H_5-NH is endothermic in the vertical pathway (15.4 kcal/mol versus −1.5 kcal/mol in the parallel route), suggesting that aniline formation would be more difficult in this orientation.

In summary, the data in Table 1 and Figs. 5 and 6 that have been discussed in this Section 3.1.4 indicate that the reduction of nitrobenzene on Ni(1 1 1) follows a four step pathway that includes the formation of nitrosobenzene C_6H_5-NO as a primary reaction intermediate, its subsequent deoxygenation yielding a stable Ph-N species, and two consecutive hydrogen transfers to N to finally produce aniline that are the most energy demanding steps of the reaction. This proposed mechanism implies that the two oxygen atoms initially present in nitrobenzene and detached from the nitro group in the course of the reaction are released to the Ni surface, and they should be removed to close the catalytic cycle and avoid catalyst oxidation and/or deactivation.

3.1.5. Water formation

Because the reducing agent is molecular H_2, the straightforward route to remove atomic oxygen from the catalyst surface is via formation and subsequent desorption of water. To our knowledge, there are no references in the literature taking into account the effect of this elementary step on the whole hydrogenation process, and therefore it has been now included in the present study.

The initial reactant system for this process contains one oxygen and two hydrogen atoms occupying hollow sites on the Ni(1 1 1) surface (see Fig. 7). In a first step, one hydrogen atom reacts with the oxygen atom to form a hydroxyl group adsorbed on a hollow site. The calculated activation energy is 21.5 kcal/mol and the

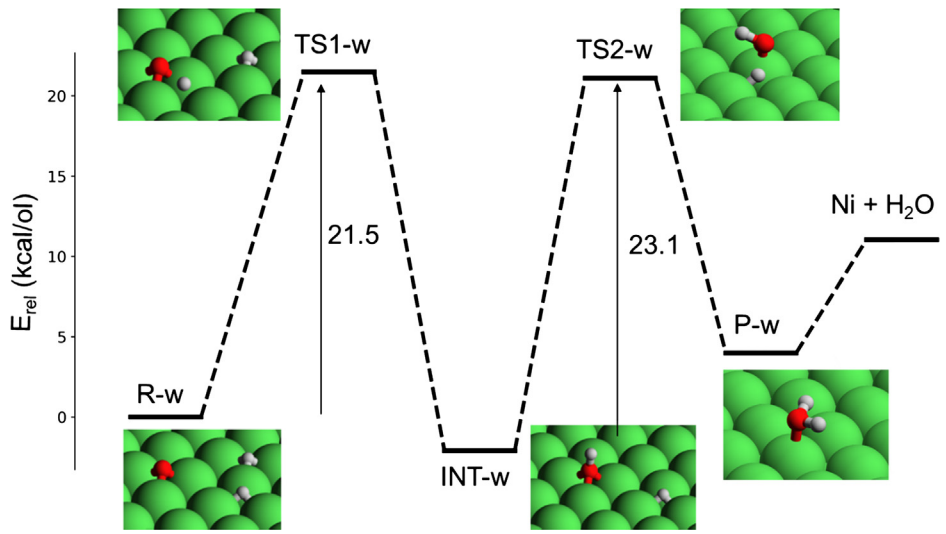

Fig. 7. Optimized structures and calculated energy profile for the formation of water from atomic H and O adsorbed on a Ni(1 1 1) surface.

reaction is exothermic by 2.1 kcal/mol (see Table S7). In a second step, another hydrogen atom reacts with the hydroxyl group that is simultaneously displaced from the hollow to a top position, finally yielding water adsorbed on top of a Ni atom (structure P-w in Fig. 7). The activation and reaction energies for this second step are 23.2 and 6.1 kcal/mol, respectively, and the final desorption of water from the surface requires 7.0 kcal/mol.

It should be noted that the activation barriers involved in the formation of water are slightly higher than those obtained for the rate-determining step of the reduction of the nitro group, suggesting that removal of oxygen and hydroxyl species from the Ni surface is not easy. The equilibrium K_{eq} and kinetic rate k_r constants summarized in Table S8 indicate that high temperature (293 K) is needed to start to form and desorb water from the catalyst surface.

3.1.6. Equilibrium and kinetic rate constants for nitrobenzene reduction

To have a more quantitative description of the mechanism of nitrobenzene hydrogenation under reaction conditions, equilibrium K_{eq} and kinetic rate k_r constants were calculated at 293 and 393 K for all steps involved in nitrobenzene hydrogenation, and are summarized in Table 2. In accordance with the energy profiles shown in Figs. 5 and 6, the dissociation of the N—O bond in nitrobenzene yielding nitrosobenzene (1 → 4) is 5–10 orders of magnitude faster than the first protonation step (1 → 2), and thermodynamically preferred by a factor larger than 10^{17}. The second N—O dissociation yielding the C_6H_5-N intermediate is also kinetically and thermodynamically favorable at high and low temperatures, with calculated K_{eq} constants in the 10^{12}–10^{28} range. These values strongly support the proposal that, on Ni catalysts, at difference with noble-metal catalysts, the mechanism of nitrobenzene hydrogenation starts with a rapid deoxygenation of the reactant.

The calculated kinetic rate k_r constants for steps 6 → 8 and 8 → 9 indicate that hydrogenation of the C_6H_5-N intermediate is the rate determining step, with calculated k_r values of only 1–20 s^{-1} at 393 K. Moreover, the low stability of C_6H_5-NH in the vertical orientation results in an extremely low K_{eq} value for step 6 → 8 even at high temperature, suggesting that if vertical C_6H_5-N species is formed it will remain adsorbed on the catalyst surface blocking the active sites unless high H_2 pressures are used. In fact, removal of adsorbed O atoms via water formation is less favored than hydrogenation of 6 in the parallel orientation, but easier than hydrogenation of 6 vertically adsorbed (see Tables 2 and S8).

In the case of nitrostyrene reduction following the parallel pathway, selectivity will depend on the relative rates of hydrogenation of the C=C bond and the nitro group, which are assimilated in this work to the rates of hydrogenation of styrene and the P6 intermediate. At 293 K the calculated rate constants k_r for styrene hydrogenation are ~10^4 times larger than those for P6 hydrogenation (see Tables 2 and S5), but the equilibrium constants follow the reverse ordering, and therefore both groups might be hydrogenated to a similar extent. Yet, Liu et al. [18] reported that Ni@C particles catalyze the hydrogenation of 3-nitrostyrene to 3-vinylaniline with selectivity above 80% using H_2 as reducing agent, which means that other pathways are being followed. Taking into account that the parallel adsorption of nitrostyrene on the Ni surface becomes more difficult in the presence of other adsorbed species (Table S3), it is possible that an increasing amount of reactant molecules adsorb in perpendicular fashion as the catalyst surface becomes covered either by the highly stable C_6H_5-N intermediate, by oxygen atoms released during the reaction, or by hydrogen atoms at high H_2 pressures, with the corresponding improvement in selectivity. A quantitative determination of the relative amount of each of these adsorbed species by means of microkinetic modelling is out of the scope of these work, but some of the main conclusions are experimentally confirmed in the following section.

3.2. Experimental study

3.2.1. Catalytic performance of Ni@C

To confirm the proposed mechanism and the trends predicted by the theoretical study, the catalytic activity and selectivity of Ni@C particles described previously by some of us [18] was measured under different reaction conditions as described in Section 2. At 20 °C nitrobenzene reacts slowly producing exclusively nitrosobenzene as a primary product (see Fig. 8a) which, after a period of about one hour, starts to be converted into aniline, as proposed by the DFT study. At full nitrobenzene conversion the selectivity to aniline is only 60%, which means that 40% of nitrosobenzene initially formed has not reacted yet, in agreement with the higher activation barriers obtained for the final hydrogenation steps leading to aniline in the theoretical part of the work. Raising the reaction temperature to 120 °C (see Fig. 8b) accelerates the process (notice the different amount of catalyst used at 20 °C and at 120 °C, see caption of Fig. 8), and the selectivity to nitrosobenzene during the first ten minutes does not exceed 60% while that of aniline is above 40%. Nitrosobenzene is then rapidly

Table 2
Calculated kinetic rate constants k_r and equilibrium constants K_{eq} at 293 and 393 K for all elementary steps of the reduction of nitrobenzene on a Ni(1 1 1) surface with parallel (P) and vertical (V) geometries.

	Parallel				Vertical			
	$k_{r(293)}$	$K_{eq(293)}$	$k_{r(393)}$	$K_{eq(393)}$	$k_{r(293)}$	$K_{eq(293)}$	$k_{r(393)}$	$K_{eq(393)}$
1 → 2	8.00×10^{2}	8.48×10^{0}	4.16×10^{5}	$5.50E \times 10^{0}$	1.55×10^{-5}	5.64×10^{-17}	6.76×10^{-1}	1.18×10^{-12}
2 → 3	9.70×10^{-3}	7.33×10^{-9}	8.93×10^{1}	1.14×10^{-6}	2.03×10^{-1}	2.43×10^{-2}	6.34×10^{2}	5.12×10^{-2}
3 → 5	2.67×10^{9}	2.04×10^{26}	1.70×10^{10}	5.46×10^{19}	8.41×10^{9}	8.80×10^{24}	3.68×10^{10}	1.13×10^{19}
2 → 5	2.38×10^{7}	1.72×10^{21}	5.96×10^{8}	7.70×10^{15}				
5 → 6	3.30×10^{8}	$1.70E \times 10^{22}$	4.09×10^{9}	4.20×10^{16}				
5 → 7	1.00×10^{-7}	9.82×10^{-9}	2.27×10^{-2}	6.06×10^{-6}	1.60×10^{-5}	9.57×10^{-6}	7.69×10^{-1}	1.99×10^{-4}
6 → 8	3.69×10^{-4}	1.19×10^{1}	1.89×10^{1}	6.36×10^{0}	4.51×10^{-5}	5.16×10^{-12}	1.01×10^{0}	5.04×10^{-9}
7 → 8	9.35×10^{4}	4.93×10^{23}	7.32×10^{6}	1.09×10^{18}	$1,28 \times 10^{10}$	1.79×10^{25}	9.46×10^{10}	2.72×10^{19}
8 → 9	1.93×10^{-3}	4.02×10^{-2}	3.57×10^{1}	1.15×10^{-1}	$1,56 \times 10^{-2}$	5.84×10^{0}	1.06×10^{2}	5.46×10^{0}
1 → 4	3.38×10^{7}	1.69×10^{23}	1.03×10^{9}	1.44×10^{17}	1.73×10^{5}	1.66×10^{12}	1.14×10^{7}	4.45×10^{9}
4 → 5	5.07×10^{0}	3.38×10^{-6}	6.54×10^{3}	8.33×10^{-5}	6.78×10^{-3}	7.27×10^{-6}	5.37×10^{1}	1.54×10^{-4}
4 → 6	5.74×10^{1}	5.76×10^{16}	2.96×10^{4}	3.50×10^{12}	1.22×10^{7}	1.80×10^{28}	3.20×10^{8}	6.81×10^{20}
4 → 10	2.27×10^{-3}	3.34×10^{-4}	2.74×10^{1}	2.21×10^{-3}				
10 → 7	2.13×10^{0}	4.65×10^{-6}	4.98×10^{3}	2.03×10^{-4}				
10 → 8	6.03×10^{7}	1.29×10^{26}	1.49×10^{9}	3.52×10^{19}				

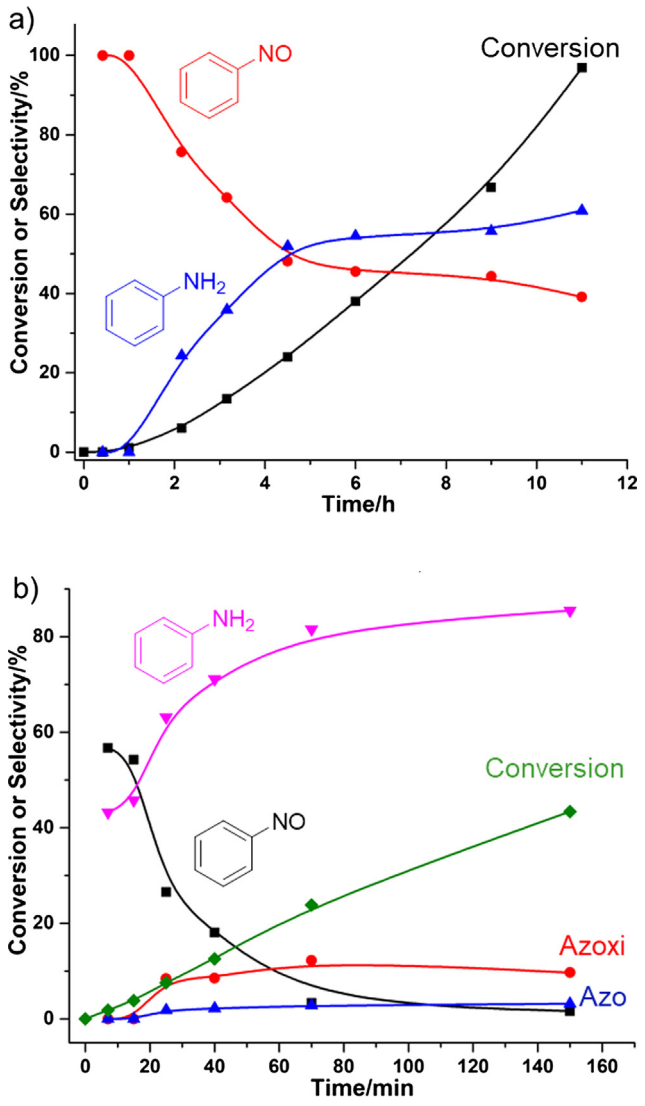

Fig. 8. Hydrogenation of nitrobenzene with Ni@C catalysts at (a) 20 °C and (b) 120 °C. Reaction conditions: 5 mg (a) and 1.5 mg (b) Ni@C as catalyst, 1 mmol 3-nitrostyrene, 2 mL toluene as solvent, 10 bar H_2.

converted into aniline, so that at 45% nitrobenzene conversion the concentration of the primary product nitrosobenzene is negligible, and the selectivity to aniline is above 85%. After 7 h reaction, at full nitrobenzene conversion, the selectivity to aniline is 100% (not shown in the plot in Fig. 8b).

Noticeably, the presence of a non-negligible amount (~10% selectivity at 45% nitrobenzene conversion) of the azoxy compound formed as intermediate in the condensation route (see Scheme 1) is also observed. The observation of a low amount of this compound only at high temperature is in line with the previous indication that the direct route is the preferred, but not the only pathway for nitrobenzene hydrogenation on Ni(1 1 1) surface [26]. This finding allows us to predict that Ni based catalysts could be adequate for producing the most difficult to obtain azoxy compounds in higher selectivity, and research work on this line is in progress.

The same catalytic behavior is observed at 120 °C when the reactant is changed to nitrostyrene, which contains two reducible groups, —NO_2 and C=C (see Fig. 9). As previously reported [18], and now confirmed with measurements under similar reaction conditions, nitrosostyrene and aminostyrene are observed from the beginning of the reaction, with the selectivity to the former

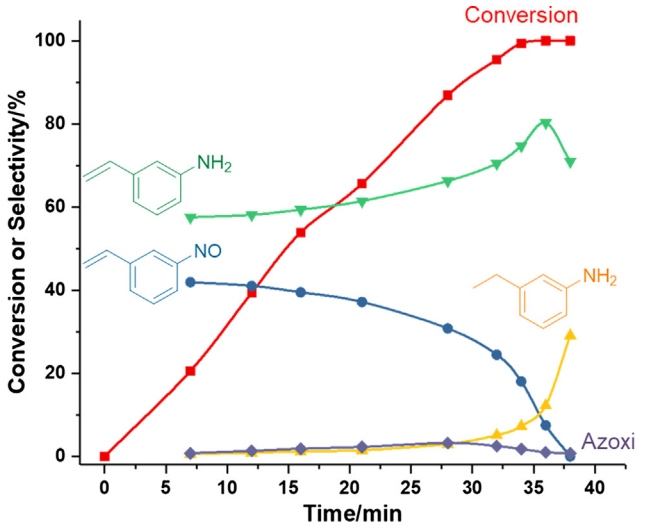

Fig. 9. Hydrogenation of nitrostyrene on Ni@C catalyst. Reaction conditions: 5 mg Ni@C as catalyst, 1 mmol 3-nitrostyrene, 2 mL toluene as solvent, 10 bar H_2 at 120 °C.

decreasing while the selectivity to the latter is increasing. It should be remarked that only at full nitrostyrene conversion, the fully hydrogenated product aminoethylbenzene starts to be formed rapidly by hydrogenation of the C=C bond of aminostyrene, causing a decrease in the total selectivity towards the desired unsaturated aminoaromatic. The reason is that when the amino group interacts with the Ni(1 1 1) surface, the aromatic ring is not oriented perpendicular to the surface but clearly bent (see Fig. 4, structure V-9), so that any reducible group present in the molecule could be attacked by surface H atoms. Since the adsorption energy of nitrobenzene (−19.1 kcal/mol in the vertical orientation) competes favorably with that of aniline (−13.3 kcal/mol), it can be assumed that the surface coverage by aniline will be low until most of the nitrobenzene has been consumed. At this moment it is feasible that the substituted aminoaromatic product adsorbed on the catalyst surface is further hydrogenated.

To test this hypothesis, competitive hydrogenation with an equimolecular mixture of nitrostyrene and aminostyrene was carried out with Ni@C at 120 °C. The results in Fig. S3 show that aminostyrene is not hydrogenated until most nitrostyrene has been converted. It is clearly shown that the formation rate of aminoethylbenzene is accelerated with the conversion of nitrostyrene, confirming that if there is a competitive adsorption of aminostyrene with nitrostyrene on the Ni@C surface this can cause a decrease of chemoselectivity.

3.2.2. Kinetic study

A kinetic study was performed to determine the rate controlling step of the process and check the hypothesis proposed from the theoretical study. For this purpose initial reaction rates for nitrobenzene hydrogenation on Ni@C were measured at different H_2 pressures (Fig. 10a) and at different nitrobenzene concentrations (Fig. 10b) working at conversion levels below 15%. According to the Hougen-Watson/Langmuir-Hinshelwood formalism, the kinetic behavior of heterogeneously catalyzed reactions can be described by different reaction rate equations depending on the rate-limiting step of the process. In the case of nitrobenzene hydrogenation on a catalyst containing just one type of active site, and assuming that both reactants adsorb on the catalyst surface before reacting, three different kinetic equations are obtained [6]. If the rate determining step is H_2 dissociation, the reaction rate is described by:

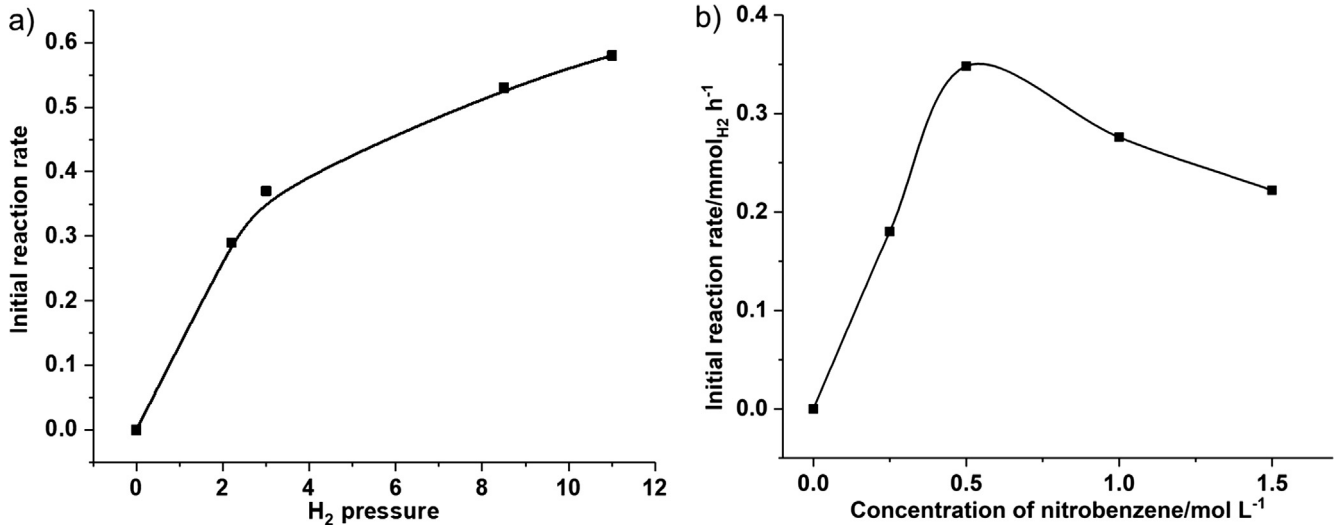

Fig. 10. Kinetic studies on hydrogenation of nitrobenzene with Ni@C nanoparticles. (a) Initial reaction rate at different H_2 pressure and 1 mmol nitrobenzene. (b) Initial reaction rate at different concentration of nitrobenzene and 11 bar of H_2. Reaction conditions: 5 mg Ni@C as catalyst, 2 mL toluene as solvent, 20 °C. The catalyst was pre-reduced at 150 °C with 10 bar of H_2 and then cooled down to 20 °C temperature before injecting the nitrobenzene to the batch reactor.

$$r = \frac{k_{H_2} \cdot P_{H_2}}{(1 + K_{NB} \cdot C_{NB})^2}$$

When nitrobenzene adsorption or activation is the step controlling the global process, then the reaction rate equation is:

$$r = \frac{k_{NB} \cdot C_{NB}}{(1 + \sqrt{K_{H_2} \cdot P_{H_2}})}$$

Finally, if the rate determining step is a surface reaction between the two reactants adsorbed on the catalyst, the kinetic equation describing the reaction rate is:

$$= \frac{k \cdot k_{NB} \cdot k_{H_2} \cdot C_{NB} \cdot P_{H_2}}{\left(1 + K_{NB} \cdot C_{NB} + \sqrt{K_{H_2} \cdot P_{H_2}}\right)^3}$$

where P_{H_2} is the H_2 pressure, C_{NB} is the concentration of nitrobenzene, k_{H_2}, k_{NB} and k are the kinetic constants of H_2 dissociation, NB adsorption and surface reaction, respectively, and K_{H_2} and K_{NB} are the equilibrium adsorption constants of H_2 and NB. The graphical representation of these three equations is plotted in Fig. S4.

A non-linear correlation between initial reaction rate and H_2 pressure is observed in Fig. 10a, while Fig. 10b shows an initial fast increase in the reaction rate with increasing NB concentration followed by a slow decrease at higher NB concentration. Comparison of the experimental results in Fig. 10 with the graphs in Fig. S4 clearly indicate that the rate determining step of the reaction is not H_2 dissociation nor NB adsorption or activation, but a hydrogenation step involving the surface reaction of hydrogen with an adsorbed intermediate. These results agree with the mechanism proposed by the theoretical study, according to which the rate determining step is the hydrogen transfer to the Ph-N intermediate adsorbed on the Ni surface.

4. Conclusions

The hydrogenation of styrene and nitrobenzene, as substrate models for the reduction of vinyl and nitro groups in nitrostyrene, respectively, have been exhaustively investigated using DFT methods. The first remarkable conclusion obtained is that nitrobenzene hydrogenation follows different pathways on noble and non-noble metals. On Pt(1 1 1), hydrogen transfer steps are easier than NO bond breaking and therefore the preferred pathway is Ph-NO_2 → Ph-NOOH → Ph-$N(OH)_2$ → Ph-NOH → Ph-NHOH → Ph-NH → Ph-NH_2, with the selectivity to substituted anilines being usually low due to the instability of the vertical adsorption orientation. In contrast, the oxophylic character of non-noble metals like Ni strongly facilitates the dissociation of the N—O bond, so that the preferred pathway for nitrobenzene reduction on Ni(1 1 1) is Ph-NO_2 → Ph-NO → Ph-N → Ph-NH → Ph-NH_2. Nitrosobenzene is formed as a primary reaction intermediate, and the rate determining step of the process is the hydrogen transfer to the highly stable Ph-N species. Both statements have been experimentally confirmed using Ni@C particles as catalyst.

The theoretical study of the reaction mechanism also shows that the oxygen atoms initially present in nitrobenzene are released to the Ni surface in the course of the reaction, and that their removal by means of water formation through reaction with activated H_2 is energetically very demanding. This provokes a partial oxidation of the Ni surface which, in turn, favors the vertical adsorption of the nitro compound, thus hindering the hydrogenation of other reducible groups present in substituted nitroaromatics and enhancing the selectivity to substituted anilines. A similar positive effect on selectivity, but detrimental on activity, is caused by the presence of the highly stable Ph-N intermediate, which blocks part of the catalyst surface and makes difficult the parallel adsorption of reactants.

It can then be concluded that both the catalytic activity and the selectivity of Ni, and maybe of other non-noble metals, can be tuned by controlling the degree of oxidation of the metal surface. Partial oxidation favors the vertical adsorption of the nitroaromatic thus enhancing selectivity, while total oxidation leads to catalyst deactivation. Based on these findings, further work is in progress to optimize the catalyst composition and the reaction conditions on other non-noble metals.

Acknowledgement

This work has been supported by the Spanish Government through "Severo Ochoa Program" (SEV-2016-0683) and by Generalitat Valenciana through AICO/2017/153 Project. Red Española de Supercomputación (RES) and Centre de Càlcul de la Universitat de Valencia are gratefully acknowledged for computational resources and technical support. The authors also thank the Microscopy Service of UPV for kind help on measurements. R. M.

acknowledges “La Caixa – Severo Ochoa” International PhD Fellowships (call 2015). L. L. thanks ITQ for providing a PhD scolarship.

Appendix A. Supplementary material

Supplementary data associated with this article can be found, in the online version, at https://doi.org/10.1016/j.jcat.2018.05.004.

References

[1] H.U. Blaser, U. Siegrist, H. Steiner, Aromatic Nitro Compounds: Fine Chemicals through Heterogeneous Catalysis, Wiley-VCH, Weinheim, Germany, 2001.
[2] H.-U. Blaser, H. Steiner, M. Studer, ChemCatChem 1 (2) (2009) 210–221.
[3] A.M. Tafesh, J. Weiguny, Chem. Rev. 96 (6) (1996) 2035–2052.
[4] A. Corma, P. Serna, Science 313 (5785) (2006) 332–334.
[5] M. Boronat, P. Concepción, A. Corma, S. González, F. Illas, P. Serna, J. Am. Chem. Soc. 129 (51) (2007) 16230–16237.
[6] P. Serna, P. Concepción, A. Corma, J. Catal. 265 (2009) 19–25.
[7] M. Boronat, A. Corma, Langmuir 26 (21) (2010) 16607–16614.
[8] P. Serna, M. Boronat, A. Corma, Top. Catal. 54 (5) (2011) 439–446.
[9] H. Wei, X. Liu, A. Wang, L. Zhang, B. Qiao, X. Yang, Y. Huang, S. Miao, J. Liu, T. Zhang, Nat. Commun. 5 (2014) 5634–5641.
[10] A. Corma, P. Serna, P. Concepción, J.J. Calvino, J. Am. Chem. Soc. 130 (27) (2008) 8748–8753.
[11] F.A. Westerhaus, R.V. Jagadeesh, G. Wienhöfer, M.-M. Pohl, J. Radnik, A.-E. Surkus, J. Rabeah, K. Junge, H. Junge, M. Nielsen, A. Brückner, M. Beller, Nat. Chem. 5 (6) (2013) 537–543.
[12] R.V. Jagadeesh, A.-E. Surkus, H. Junge, M.-M. Pohl, J. Radnik, J. Rabeah, H. Huan, V. Schünemann, A. Brückner, M. Beller, Science 342 (6162) (2013) 1073–1076.
[13] O. Beswick, A. Parastaev, I. Yuranov, T. LaGrange, P.J. Dyson, L. Kiwi-Minsker, Catal. Today 279 (2017) 29–35.
[14] Z. Wei, J. Wang, S. Mao, D. Su, H. Jin, Y. Wang, F. Xu, H. Li, Y. Wang, ACS Catal. 5 (8) (2015) 4783–4789.
[15] L. Liu, P. Concepción, A. Corma, J. Catal. 340 (2016) 1–9.
[16] G. Hahn, J.-K. Ewert, C. Denner, D. Tilgner, R. Kempe, ChemCatChem 8 (2016) 2461–2465.
[17] Y. Ren, H. Wei, G. Yin, L. Zhang, A. Wang, T. Zhang, Chem. Commun. 53 (2017) 1969–1972.
[18] L. Liu, F. Gao, P. Concepción, A. Corma, J. Catal. 350 (2017) 218–225.
[19] J. Zhang, G. Lu, C. Cai, Catal. Commun. 84 (2016) 25–29.
[20] D.R. Petkar, B.S. Kadu, R.C. Chikate, RSC Adv 4 (16) (2014) 8004–8010.
[21] F. Haber, Elektrochem. 4 (1898) 506.
[22] E.A. Gelder, S.D. Jackson, C.M. Lok, Chem. Commun. (4) (2005) 522–524.
[23] A. Corma, P. Concepción, P. Serna, Angew. Chem. Int. Ed. 46 (38) (2007) 7266–7269.
[24] T. Sheng, Y.-J. Qi, X. Lin, P. Hu, S.-G. Sun, W.-F. Lin, Chem. Eng. J. 293 (2016) 337–344.
[25] L. Zhang, J. Jiang, W. Shi, S. Xia, Z. Ni, X. Xiao, RSC Adv. 5 (43) (2015) 34319–34326.
[26] A. Mahata, R.K. Rai, I. Choudhuri, S.K. Singh, B. Pathak, Phys. Chem. Chem. Phys. 16 (47) (2014) 26365–26374.
[27] S. Furukawa, K. Takahashi, T. Komatsu, Chem. Sci. 7 (7) (2016) 4476–4484.
[28] L. Zhang, X.-M. Cao, P. Hu, Appl. Surf. Sci. 392 (2017) 456–471.
[29] J.P. Perdew, J.A. Chevary, S.H. Vosko, K.A. Jackson, M.R. Pederson, D.J. Singh, C. Fiolhais, Phys. Rev. B 46 (1992) 6671–6687.
[30] J.P. Perdew, Y. Wang, Phys. Rev. B 45 (1992) 13244–13249.
[31] G. Kresse, J. Furthmüller, Phys. Rev. B 54 (1996) 11169–11186.
[32] P.E. Blöchl, Phys. Rev. B 50 (1994) 17953–17979.
[33] G. Henkelman, H. Jónsson, J. Chem. Phys. 111 (1999) 7010–7022.
[34] A. Heyden, A.T. Bell, F.J. Keil, J. Chem. Phys. 123 (2005) 224101–224114.
[35] S. Grimme, J. Antony, S. Ehrlich, H. Krieg, J. Chem. Phys. 132 (2010) 154104.
[36] H.J. Monkhorst, J.D. Pack, Phys. Rev. B 13 (1976) 5188.
[37] P. Ferrin, S. Kandoi, A.U. Nilekar, M. Mavrikakis, Surf. Sci. 606 (2012) 679–689.
[38] K.P. Kepp, Inorg. Chem. 55 (18) (2016) 9461–9470.